Observation of χ_{c1} Decays into Vector Meson Pairs $\phi\phi$, $\omega\omega$, and $\omega\phi$

M. Ablikim,[1] M. N. Achasov,[5] L. An,[9] Q. An,[39] Z. H. An,[1] J. Z. Bai,[1] R. Baldini,[20] Y. Ban,[26] J. Becker,[2] N. Berger,[1] M. Bertani,[20] J. M. Bian,[1] O. Bondarenko,[19] I. Boyko,[15] R. A. Briere,[3] V. Bytev,[15] X. Cai,[1] G. F. Cao,[1] X. X. Cao,[1] J. F. Chang,[1] G. Chelkov,[16] G. Chen,[1] H. S. Chen,[1] J. C. Chen,[1] M. L. Chen,[1] S. J. Chen,[24] Y. Chen,[1] Y. B. Chen,[1] H. P. Cheng,[11] Y. P. Chu,[1] D. Cronin-Hennessy,[38] H. L. Dai,[1] J. P. Dai,[1] D. Dedovich,[15] Z. Y. Deng,[1] I. Denysenko,[17] M. Destefanis,[41] Y. Ding,[22] L. Y. Dong,[1] M. Y. Dong,[1] S. X. Du,[45] M. Y. Duan,[29] R. R. Fan,[1] J. Fang,[1] S. S. Fang,[1] C. Q. Feng,[39] C. D. Fu,[1] J. L. Fu,[24] Y. Gao,[35] C. Geng,[39] K. Goetzen,[7] W. X. Gong,[1] M. Greco,[41] S. Grishin,[15] M. H. Gu,[1] Y. T. Gu,[9] Y. H. Guan,[6] A. Q. Guo,[25] L. B. Guo,[23] Y. P. Guo,[25] X. Q. Hao,[1] F. A. Harris,[37] K. L. He,[1] M. He,[1] Z. Y. He,[25] Y. K. Heng,[1] Z. L. Hou,[1] H. M. Hu,[1] J. F. Hu,[6] T. Hu,[1] B. Huang,[1] G. M. Huang,[12] J. S. Huang,[10] X. T. Huang,[28] Y. P. Huang,[1] T. Hussain,[40] C. S. Ji,[39] Q. Ji,[1] X. B. Ji,[1] X. L. Ji,[1] L. K. Jia,[1] L. L. Jiang,[1] X. S. Jiang,[1] J. B. Jiao,[28] Z. Jiao,[11] D. P. Jin,[1] S. Jin,[1] F. F. Jing,[35] M. Kavatsyuk,[19] S. Komamiya,[34] W. Kuehn,[36] J. S. Lange,[36] J. K. C. Leung,[33] Cheng Li,[39] Cui Li,[39] D. M. Li,[45] F. Li,[1] G. Li,[1] H. B. Li,[1] J. C. Li,[1] Lei Li,[1] N. B. Li,[23] Q. J. Li,[1] W. D. Li,[1] W. G. Li,[1] X. L. Li,[28] X. N. Li,[1] X. Q. Li,[25] X. R. Li,[1] Z. B. Li,[31] H. Liang,[39] Y. F. Liang,[30] Y. T. Liang,[36] G. R. Liao,[8] X. T. Liao,[1] B. J. Liu,[33] B. J. Liu,[32] C. L. Liu,[3] C. X. Liu,[1] C. Y. Liu,[1] F. H. Liu,[29] Fang Liu,[1] Feng Liu,[12] G. C. Liu,[1] H. Liu,[1] H. B. Liu,[6] H. M. Liu,[1] H. W. Liu,[1] J. P. Liu,[43] K. Liu,[26] K. Y. Liu,[22] Q. Liu,[37] S. B. Liu,[39] X. Liu,[21] X. H. Liu,[1] Y. B. Liu,[25] Y. W. Liu,[39] Yong Liu,[1] Z. A. Liu,[1] Z. Q. Liu,[1] H. Loehner,[19] G. R. Lu,[10] H. J. Lu,[11] J. G. Lu,[1] Q. W. Lu,[29] X. R. Lu,[6] Y. P. Lu,[1] C. L. Luo,[23] M. X. Luo,[44] T. Luo,[1] X. L. Luo,[1] C. L. Ma,[6] F. C. Ma,[22] H. L. Ma,[1] Q. M. Ma,[1] T. Ma,[1] X. Ma,[1] X. Y. Ma,[1] M. Maggiora,[41] Q. A. Malik,[40] H. Mao,[1] Y. J. Mao,[26] Z. P. Mao,[1] J. G. Messchendorp,[19] J. Min,[1] R. E. Mitchell,[14] X. H. Mo,[1] N. Yu. Muchnoi,[5] Y. Nefedov,[15] Z. Ning,[1] S. L. Olsen,[27] Q. Ouyang,[1] S. Pacetti,[20] M. Pelizaeus,[37] K. Peters,[7] J. L. Ping,[23] R. G. Ping,[1] R. Poling,[38] C. S. J. Pun,[33] M. Qi,[24] S. Qian,[1] C. F. Qiao,[6] X. S. Qin,[1] J. F. Qiu,[1] K. H. Rashid,[40] G. Rong,[1] X. D. Ruan,[9] A. Sarantsev,[18] J. Schulze,[2] M. Shao,[39] C. P. Shen,[37] X. Y. Shen,[1] H. Y. Sheng,[1] M. R. Shepherd,[14] X. Y. Song,[1] S. Sonoda,[34] S. Spataro,[41] B. Spruck,[36] D. H. Sun,[1] G. X. Sun,[1] J. F. Sun,[10] S. S. Sun,[1] X. D. Sun,[1] Y. J. Sun,[39] Y. Z. Sun,[1] Z. J. Sun,[1] Z. T. Sun,[39] C. J. Tang,[30] X. Tang,[1] X. F. Tang,[8] H. L. Tian,[1] D. Toth,[38] G. S. Varner,[37] X. Wan,[1] B. Q. Wang,[26] K. Wang,[1] L. L. Wang,[4] L. S. Wang,[1] M. Wang,[28] P. Wang,[1] P. L. Wang,[1] Q. Wang,[1] S. G. Wang,[26] X. L. Wang,[39] Y. D. Wang,[39] Y. F. Wang,[1] Y. Q. Wang,[28] Z. Wang,[1] Z. G. Wang,[1] Z. Y. Wang,[1] D. H. Wei,[8] Q. G. Wen,[39] S. P. Wen,[1] U. Wiedner,[2] L. H. Wu,[1] N. Wu,[1] W. Wu,[22] Z. Wu,[1] Z. J. Xiao,[23] Y. G. Xie,[1] G. F. Xu,[1] G. M. Xu,[26] H. Xu,[1] Y. Xu,[25] Z. R. Xu,[39] Z. Z. Xu,[39] Z. Xue,[1] L. Yan,[39] W. B. Yan,[39] Y. H. Yan,[13] H. X. Yang,[1] M. Yang,[1] T. Yang,[9] Y. Yang,[12] Y. X. Yang,[8] M. Ye,[1] M. H. Ye,[4] B. X. Yu,[1] C. X. Yu,[25] L. Yu,[12] C. Z. Yuan,[1] W. L. Yuan,[23] Y. Yuan,[1] A. A. Zafar,[40] A. Zallo,[20] Y. Zeng,[13] B. X. Zhang,[1] B. Y. Zhang,[1] C. C. Zhang,[1] D. H. Zhang,[1] H. H. Zhang,[31] H. Y. Zhang,[1] J. Zhang,[23] J. W. Zhang,[1] J. Y. Zhang,[1] J. Z. Zhang,[1] L. Zhang,[24] S. H. Zhang,[1] T. R. Zhang,[23] X. J. Zhang,[1] X. Y. Zhang,[28] Y. Zhang,[1] Y. H. Zhang,[1] Z. P. Zhang,[39] Z. Y. Zhang,[43] G. Zhao,[1] H. S. Zhao,[1] Jiawei Zhao,[39] Jingwei Zhao,[1] Lei Zhao,[39] Ling Zhao,[1] M. G. Zhao,[25] Q. Zhao,[1] S. J. Zhao,[45] T. C. Zhao,[42] X. H. Zhao,[24] Y. B. Zhao,[1] Z. G. Zhao,[39] Z. L. Zhao,[9] A. Zhemchugov,[16] B. Zheng,[1] J. P. Zheng,[1] Y. H. Zheng,[6] Z. P. Zheng,[1] B. Zhong,[1] J. Zhong,[2] L. Zhong,[35] L. Zhou,[1] X. K. Zhou,[6] X. R. Zhou,[39] C. Zhu,[1] K. Zhu,[1] K. J. Zhu,[1] S. H. Zhu,[1] X. L. Zhu,[35] X. W. Zhu,[1] Y. S. Zhu,[1] Z. A. Zhu,[1] J. Zhuang,[1] B. S. Zou,[1] J. H. Zou,[1] J. X. Zuo,[1] and P. Zweber[38]

(BESIII Collaboration)

[1]*Institute of High Energy Physics, Beijing 100049, People's Republic of China*
[2]*Bochum Ruhr-University, 44780 Bochum, Germany*
[3]*Carnegie Mellon University, Pittsburgh, Pennsylvania 15213, USA*
[4]*China Center of Advanced Science and Technology, Beijing 100190, People's Republic of China*
[5]*G.I. Budker Institute of Nuclear Physics SB RAS (BINP), Novosibirsk 630090, Russia*
[6]*Graduate University of Chinese Academy of Sciences, Beijing 100049, People's Republic of China*
[7]*GSI Helmholtzcentre for Heavy Ion Research GmbH, D-64291 Darmstadt, Germany*
[8]*Guangxi Normal University, Guilin 541004, People's Republic of China*
[9]*Guangxi University, Naning 530004, People's Republic of China*
[10]*Henan Normal University, Xinxiang 453007, People's Republic of China*
[11]*Huangshan College, Huangshan 245000, People's Republic of China*
[12]*Huazhong Normal University, Wuhan 430079, People's Republic of China*
[13]*Hunan University, Changsha 410082, People's Republic of China*
[14]*Indiana University, Bloomington, Indiana 47405, USA*

[15]Joint Institute for Nuclear Research, 141980 Dubna, Russia
[16]also at the Moscow Institute of Physics and Technology, Moscow, Russia
[17]on leave from the Bogolyubov Institute for Theoretical Physics, Kiev, Ukraine
[18]also at the PNPI, Gatchina, Russia
[19]KVI/University of Groningen, 9747 AA Groningen, The Netherlands
[20]Laboratori Nazionali di Frascati - INFN, 00044 Frascati, Italy
[21]Lanzhou University, Lanzhou 730000, People's Republic of China
[22]Liaoning University, Shenyang 110036, People's Republic of China
[23]Nanjing Normal University, Nanjing 210046, People's Republic of China
[24]Nanjing University, Nanjing 210093, People's Republic of China
[25]Nankai University, Tianjin 300071, People's Republic of China
[26]Peking University, Beijing 100871, People's Republic of China
[27]Seoul National University, Seoul, 151-747 Korea
[28]Shandong University, Jinan 250100, People's Republic of China
[29]Shanxi University, Taiyuan 030006, People's Republic of China
[30]Sichuan University, Chengdu 610064, People's Republic of China
[31]Sun Yat-Sen University, Guangzhou 510275, People's Republic of China
[32]The Chinese University of Hong Kong, Shatin, N.T., Hong Kong.
[33]The University of Hong Kong, Pokfulam, Hong Kong
[34]The University of Tokyo, Tokyo 113-0033 Japan
[35]Tsinghua University, Beijing 100084, People's Republic of China
[36]Universitaet Giessen, 35392 Giessen, Germany
[37]University of Hawaii, Honolulu, Hawaii 96822, USA
[38]University of Minnesota, Minneapolis, Minnesota 55455, USA
[39]University of Science and Technology of China, Hefei 230026, People's Republic of China
[40]University of the Punjab, Lahore-54590, Pakistan
[41]University of Turin and INFN, Turin, Italy
[42]University of Washington, Seattle, Washington 98195, USA
[43]Wuhan University, Wuhan 430072, People's Republic of China
[44]Zhejiang University, Hangzhou 310027, People's Republic of China
[45]Zhengzhou University, Zhengzhou 450001, People's Republic of China

(Received 27 April 2011; published 22 August 2011)

Using $(106 \pm 4) \times 10^6$ $\psi(3686)$ events accumulated with the BESIII detector at the BEPCII e^+e^- collider, we present the first measurement of decays of χ_{c1} to vector meson pairs $\phi\phi$, $\omega\omega$, and $\omega\phi$. The branching fractions are measured to be $(4.4 \pm 0.3 \pm 0.5) \times 10^{-4}$, $(6.0 \pm 0.3 \pm 0.7) \times 10^{-4}$, and $(2.2 \pm 0.6 \pm 0.2) \times 10^{-5}$, for $\chi_{c1} \to \phi\phi$, $\omega\omega$, and $\omega\phi$, respectively, which indicates that the hadron helicity selection rule is significantly violated in χ_{cJ} decays. In addition, the measurement of $\chi_{cJ} \to \omega\phi$ provides the first indication of the rate of doubly OZI-suppressed χ_{cJ} decay. Finally, we present improved measurements for the branching fractions of χ_{c0} and χ_{c2} to vector meson pairs.

DOI: 10.1103/PhysRevLett.107.092001 PACS numbers: 13.25.Gv, 12.38.Qk, 14.40.Pq

Decays of the $\chi_{cJ}(J = 0, 1, 2)$ P-wave charmonium states are considered to be an ideal laboratory to test QCD theory. The initial theoretical calculations of χ_{cJ} exclusive decays into light hadrons predicted branching fractions that were smaller than the experimental measurements [1]. With the inclusion of the color-octet mechanism [2], calculations of χ_{cJ} decays into pairs of pseudoscalar mesons and pairs of baryons came into reasonable agreement with the experimental measurements, indicating the importance of the color-octet mechanism.

In the case of χ_{cJ} decays into pairs of vector ($J^{PC} = 1^{--}$) mesons VV, where V is an ω or ϕ, the branching fractions for $\chi_{c0/2}$ decays to $\phi\phi$ and $\omega\omega$ have been measured to be at the 10^{-3} level [3,4], which is much larger than predictions based on perturbative QCD calculations [5]. Decays of the χ_{c1} into $\phi\phi$, $\omega\omega$ and $\omega\phi$ violate the helicity selection rule (HSR) and are expected to be highly suppressed [6]. In addition, the decays $\chi_{cJ} \to \omega\phi$ are doubly OZI suppressed and have yet to be observed. Recently, long-distance effects in χ_{c1} decays [7,8] have been proposed to account for the HSR violation. Precise measurements of $\chi_{c1} \to VV$ decays will help clarify the influence of long-distance effects in this energy region.

In this Letter, we report measurements of χ_{cJ} decays into $\phi\phi$, $\omega\omega$, and $\omega\phi$ modes, where ϕ is reconstructed from K^+K^- or $\pi^+\pi^-\pi^0$, ω from $\pi^+\pi^-\pi^0$, and π^0 from $\gamma\gamma$. The data samples used in this analysis consist of $(106 \pm 4) \times 10^6$ $\psi(3686)$ decays and 42.6 pb^{-1} of continuum data at $\sqrt{s} = 3.65$ GeV acquired with the BESIII detector [9]. The cylindrical core of the BESIII detector consists of a helium-gas-based Main Drift

Chamber (MDC), a plastic scintillator Time-of-Flight system (TOF), a CsI(Tl) Electromagnetic Calorimeter (EMC), and a muon counter. The charged particle and photon acceptance is 93% of 4π, and the charged particle momentum and photon energy resolutions at 1 GeV are 0.5% and 2.5%, respectively. The BESIII detector is modeled with a Monte Carlo (MC) simulation based on GEANT4 [10,11]. The optimization of the event selection and the estimation of physics backgrounds are performed with Monte Carlo simulations of $\psi(3686)$ inclusive or exclusive decays [12].

The final states of interest are $\gamma 2(K^+K^-)$, $5\gamma 2(\pi^+\pi^-)$, and $3\gamma K^+K^-\pi^+\pi^-$. Event candidates are required to have four well reconstructed charged tracks with net charge zero, and at least one, five, or three good photons, for $\phi\phi$, $\omega\omega$, and $\omega\phi$, respectively.

Electromagnetic showers in BESIII detector are reconstructed from clusters of energy deposits in the EMC. The energy deposited in nearby TOF counters is included to improve the reconstruction efficiency. A good photon is a shower in the barrel region ($|\cos\theta| < 0.8$) with at least 25 MeV energy deposition, or in the end caps ($0.86 < |\cos\theta| < 0.92$) with at least 50 MeV energy deposition, where θ is the polar angle of the shower. Showers in the region between the barrel and the end caps are poorly measured and excluded. Timing requirements are used in the EMC to suppress electronic noise and energy deposits unrelated to the event.

Charged tracks are reconstructed from MDC hits. Each charged track is required to be in the polar angle region $|\cos\theta| < 0.93$ and to pass within ± 10 cm of the interaction point in the beam direction and within ± 1 cm in the plane perpendicular to the beam.

A kinematic fit constrained by the initial e^+e^- four-momentum in the laboratory frame is applied to the decay hypotheses $\psi(3686) \to \gamma 2(K^+K^-)$, $5\gamma 2(\pi^+\pi^-)$, and $3\gamma K^+K^-\pi^+\pi^-$. The final state photons are identified with the photon-charged-track combination that has a minimum χ^2_{4C} value (for definition of χ^2_{4C}, see [13]) when sampling all candidate photons. The vertex of all charged tracks must be consistent with the measured beam interaction point. The χ^2_{4C} selection efficiency is optimized using the ratio of signal to backgrounds in the data: $\chi^2_{4C} < 60$ for $\gamma 2(K^+K^-)$, $3\gamma K^+K^-\pi^+\pi^-$, and $\chi^2_{4C} < 200$ for $5\gamma 2(\pi^+\pi^-)$ is required. To separate the $K^\pm$ from $\pi^\pm$ in the $3\gamma K^+K^-\pi^+\pi^-$ final state, two kaons are identified with the requirements that $P(K) > P(\pi)$ and $P(K) > P(p)$, where $P(X)$ is the probability of hypothesis X as evaluated from the TOF and dE/dx information.

The mass windows for resonance candidates are set according to the optimized ratio of signals to backgrounds in the data. The π^0 candidates are selected by requiring $0.1 < M_{\gamma\gamma} < 0.15$ GeV/c^2. The ϕ and ω candidates are selected by requiring $|M_{K^+K^-} - 1.019| < 0.015$ GeV/c^2, $|M_{\pi^+\pi^-\pi^0} - 1.019| < 0.030$ GeV/c^2, and $|M_{\pi^+\pi^-\pi^0} - 0.783| < 0.050$ GeV/c^2, for $\phi \to K^+K^-$, $\phi \to \pi^+\pi^-\pi^0$, and $\omega \to \pi^+\pi^-\pi^0$, respectively.

For $\chi_{cJ} \to \phi\phi \to 2(K^+K^-)$, the two ϕ candidates with the minimum value of $(M^{(1)}_{K^+K^-} - 1.019)^2 + (M^{(2)}_{K^+K^-} - 1.019)^2$ are taken as the signal. No artificial ϕ-pair peaks are produced when this selection criteria is applied to MC simulation of the process $\chi_{cJ} \to 2(K^+K^-)$. A scatterplot of masses for one K^+K^- pair *versus* the other K^+K^- pair is shown in Fig. 1(a), where a clear $\phi\phi$ signal can be seen. The $M_{K^+K^-}$ distribution, after requiring that the other two kaons are consistent with being a ϕ, is shown in Fig. 1(b). A ϕ peak is clearly seen with very low background. The $\phi\phi$ invariant mass distribution for the selected events is shown in Fig. 2(a), where χ_{cJ} signals are clearly observed. The MC simulation shows that the peaking backgrounds, i.e., backgrounds that produce χ_{cJ} signal peaks, are mostly from $\chi_{cJ} \to \phi K^+K^-$ and $2(K^+K^-)$ final states; the

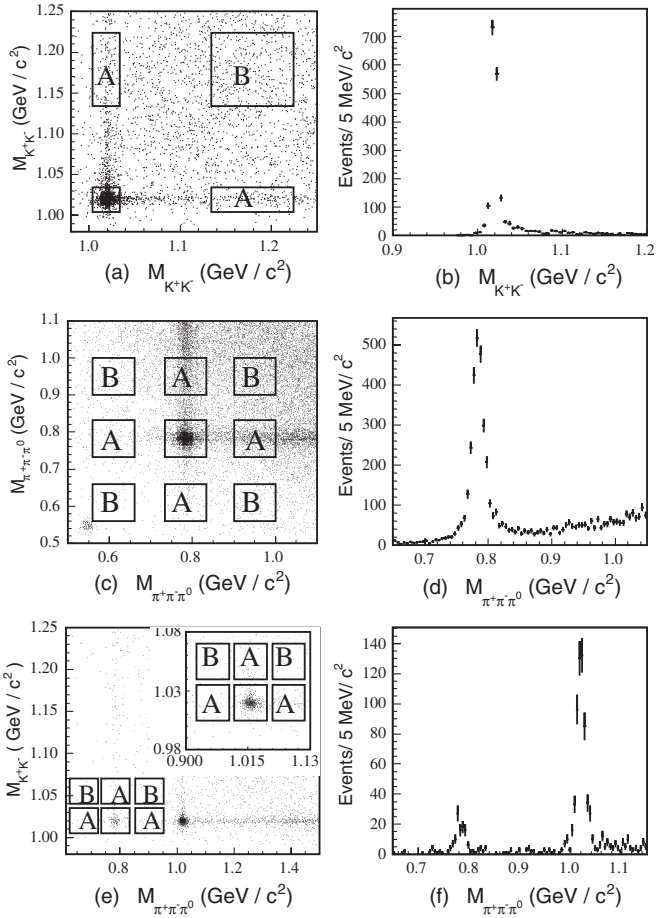

FIG. 1. The left column shows scatterplots for events within the χ_{cJ} mass region. The boxes indicate the signal region (without label) and sideband regions labeled as A and B. The plots in the right column are the one-dimensional projections of the system recoiling against a selected ϕ or ω resonance. Plots (a) and (b) are for the $\gamma 2(K^+K^-)$ mode; (c) and (d) for the $5\gamma 2(\pi^+\pi^-)$ mode; and (e) and (f) for the $3\gamma K^+K^-\pi^+\pi^-$ mode.

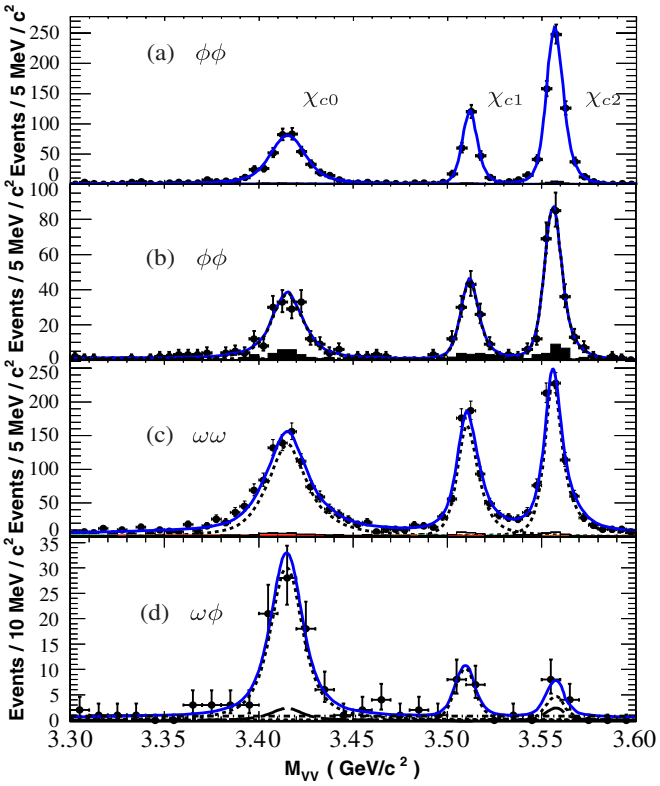

FIG. 2 (color online). Invariant mass of VV for (a) $\phi\phi$ mode in the $\gamma 2(K^+K^-)$ final state, (b) $\phi\phi$ mode in the $\gamma\pi^+\pi^-\pi^0K^+K^-$ final state, (c) $\omega\omega$ mode in the $\gamma 2(\pi^+\pi^-\pi^0)$ final state, and (d) $\omega\phi$ mode in the $\gamma\pi^+\pi^-\pi^0K^+K^-$ final state. The points with error bars are the data; the solid lines are the fit results; and dotted lines represent the signal components. The shaded and open histograms in (a),(b) and (c), respectively, are peaking backgrounds. In (c), the shaded histogram denotes the non-χ_{cJ} backgrounds. In (d) the long dash line is background normalized by a simultaneous fit to $\omega\phi$ sidebands, and the dash-dot line is non-χ_{cJ} background.

backgrounds from misidentified charged particles are negligible. The levels of the peaking backgrounds are evaluated from $N_{AB} = r_A N_A^{dt} - r_B N_B^{dt}$, where $N_A^{dt}(N_B^{dt})$ is the number of data events falling into box A (B), as indicated in Fig. 1(a), and the normalizing factors $r_i = N_{\rm sig}^{\rm MC}/N_i^{\rm MC}$ with $i = A$ or B are determined from MC simulation for modes $\chi_{cJ} \to \phi K^+K^-$ and $2(K^+K^-)$, respectively. Here $N_{\rm sig}^{\rm MC}(N_i^{\rm MC})$ is the number of MC events falling into the signal box (A or B). These backgrounds will be indistinguishable from signal events; therefore, we fix their normalization, independently for each χ_{cJ} peak, in the final fit.

To study $\chi_{cJ} \to \omega\omega$ decays into the $2(\pi^+\pi^-\pi^0)$ final state, two π^0 candidates are selected by minimizing the value of $(M_{\gamma\gamma}^{(1)} - 0.135)^2 + (M_{\gamma\gamma}^{(2)} - 0.135)^2$ when sampling all four-photon combinations from the selected five photons. The $\pi^+\pi^-\pi^0$ combination closest to the nominal ω mass is taken as one ω candidate, and the remaining three pions are assumed to be from the other ω. No artificial ω-pair peaks are produced from the application of this ω-selection criteria to a MC simulation for $\chi_{cJ} \to 2(\pi^+\pi^-\pi^0)$. A scatterplot of the mass for one $\pi^+\pi^-\pi^0$ pair *versus* the other $\pi^+\pi^-\pi^0$ pair is shown in Fig. 1(c), and the $M_{\pi^+\pi^-\pi^0}$ distribution for the three pions recoiling against an ω candidate is plotted in Fig. 1(d). The $\omega\omega$ mass spectrum is shown in Fig. 2(c), where χ_{cJ} signals are prominent. The MC simulation shows that the backgrounds in the $\omega\omega$ signal region include peaking backgrounds from $\chi_{cJ} \to \omega\pi^+\pi^-\pi^0$ and $2(\pi^+\pi^-\pi^0)$, and nonpeaking backgrounds from the $\psi(3686)$ decays into the same final states without intermediate χ_{cJ} states. The backgrounds from misidentified charged particles are negligible. Potential backgrounds from $\chi_{cJ} \to \phi\phi \to 2(\pi^+\pi^-\pi^0)$ and $\chi_{c0/2} \to \eta\eta \to 2(\pi^+\pi^-\pi^0)$ do not survive our selection criteria. As in the $\chi_{cJ} \to \phi\phi$ mode, the sizes of the peaking backgrounds from $\chi_{cJ} \to \omega\pi^+\pi^-\pi^0$ and $2(\pi^+\pi^-\pi^0)$ are evaluated by selecting data events located in sideband boxes A and B, respectively, as indicated in Fig. 1(c). The peaking backgrounds are normalized according to the ratio of MC events falling into the signal region and those falling into the sidebands. The normalization of these peaking backgrounds is fixed in the final fit.

To study $\chi_{cJ} \to \omega\phi$ and $\phi\phi$ decays into the $K^+K^-\pi^+\pi^-\pi^0$ final state, the photon pair with invariant mass closest to the π^0 nominal mass is taken as the π^0 candidate. A scatterplot of masses for K^+K^- pairs *versus* that for $\pi^+\pi^-\pi^0$ pairs is shown in Fig. 1(e), and the $M_{\pi^+\pi^-\pi^0}$ distribution for events satisfying $\phi \to K^+K^-$ is shown in Fig. 1(f), where the $\omega \to \pi^+\pi^-\pi^0$ and $\phi \to \pi^+\pi^-\pi^0$ signals are clearly seen. The $\phi\phi$ and $\omega\phi$ mass spectra are shown in Figs. 2(b) and 2(d), respectively. Similar to the case for $\chi_{cJ} \to \phi\phi \to 2(K^+K^-)$, the peaking backgrounds from the $\chi_{cJ} \to \phi\pi^+\pi^-\pi^0$ or ϕK^+K^-, and $K^+K^-\pi^+\pi^-\pi^0$ are evaluated by selecting data events falling into sideband boxes A and B, respectively, as indicated in the inserted plot in Fig. 1(e). The peaking backgrounds are normalized according to the ratio of MC events falling into the signal region and those falling into the sidebands. The normalization of these peaking backgrounds is fixed in the final fit.

The numbers of observed events are obtained by fitting the M_{VV} distributions. The observed line shapes are described with modified χ_{cJ} MC shapes plus backgrounds. Possible interference effects between the signal mode and the peaking background modes are not considered for all modes. The original χ_{cJ} MC shapes are generated by a relativistic Breit-Wigner incorporated with full helicity amplitudes in the EvtGen package [14], and their masses and widths are set to the nominal values [15]. In the fits they are modified by convolving them with Gaussian functions $G(M_{VV} - \delta M_J, \sigma_J)$, where δM_J and σ_J correct the χ_{cJ} mass and width or resolution, respectively, in the simulation. The values of δM_J and σ_J, determined from

the fits, are less than 1 MeV for all modes and from 1 to 5 MeV, respectively. Backgrounds from QED processes, which are estimated from the application of a similar analysis to the continuum data, are negligible. For $\chi_{cJ} \to \phi\phi$, the peaking backgrounds are fixed to the sideband estimates as mentioned above, and other combinatorial backgrounds are parameterized by a second-order polynomial with parameters that are allowed to float in the fit. For all modes, a maximum-likelihood technique [16] is employed to estimate parameters. After projecting the best fit into the binned histograms shown in Fig. 2, we determine $\chi^2/\mathrm{NDF} = 0.46$ for $\chi_{cJ} \to \phi\phi \to 2(K^+K^-)$ and 0.50 for the $\chi_{cJ} \to \phi\phi \to K^+K^-\pi^+\pi^-\pi^0$, where NDF is the number of degrees of freedom. The fitted results are plotted in Fig. 2(a) and 2(b), respectively. The numbers of signal events are listed in Table I.

For the $\chi_{cJ} \to \omega\omega$ channel, backgrounds include the peaking backgrounds estimated from ω sidebands indicated in Fig. 1(c), non-χ_{cJ} backgrounds [$\psi(3686) \to \gamma\omega\omega$] fixed at the normalized MC shape of phase space using the data information, and smooth combinatorial backgrounds that are parametrized by a second-order polynomial. The χ^2/NDF for the fit is 0.97. The fit results are shown in Fig. 2(c).

To extract the signal yield, as well as to estimate the statistical significance for the $\chi_{cJ} \to \omega\phi$ mode, a simultaneous fit is performed to $M_{\omega\phi}$ distributions both in $\omega\phi$ signal and sideband regions of boxes A and B [see Fig. 1(e)]. The peaking backgrounds are normalized according to the ratio of MC events falling into the signal region to those falling into the sideband regions for the $\psi(3686) \to \gamma\phi\pi^+\pi^-\pi^0$, $\gamma\omega K^+K^-$ and $\psi(3686) \to \gamma K^+K^-\pi^+\pi^-\pi^0$ events that are within the χ_{cJ} mass region. Because of the low signal yield in this mode, the parameters δM_J and σ_J of the modified MC shapes are fixed at the values determined in the fit of $\chi_{cJ} \to \phi\phi \to K^+K^-\pi^+\pi^-\pi^0$. The χ^2/NDF is 0.62. The fit results are shown in Fig. 2(d), and the numbers of signal events are listed in Table I.

TABLE I. Summary of the branching fractions ($\mathcal{B}$) for $\chi_{cJ} \to \phi\phi$, $\omega\omega$, and $\omega\phi$. Here N_{net} is the number of signal events, ϵ is the detection efficiency. The upper limit is estimated at the 90% C.L.

Mode	N_{net}	ϵ (%)	$\mathcal{B}(\times 10^{-4})$
$\chi_{c0} \to \phi\phi$	433 ± 23	22.4	$7.8 \pm 0.4 \pm 0.8$
$\chi_{c1} \to \phi\phi$	254 ± 17	26.4	$4.1 \pm 0.3 \pm 0.4$
$\chi_{c2} \to \phi\phi \to 2(K^+K^-)$	630 ± 26	26.1	$10.7 \pm 0.4 \pm 1.1$
$\chi_{c0} \to \phi\phi$	179 ± 16	12.8	$9.2 \pm 0.7 \pm 1.0$
$\chi_{c1} \to \phi\phi$	112 ± 12	15.3	$5.0 \pm 0.5 \pm 0.6$
$\chi_{c2} \to \phi\phi \to K^+K^-\pi^+\pi^-\pi^0$	219 ± 16	14.9	$10.7 \pm 0.7 \pm 1.2$
Combined:			
$\chi_{c0} \to \phi\phi$	...	...	$8.0 \pm 0.3 \pm 0.8$
$\chi_{c1} \to \phi\phi$	...	...	$4.4 \pm 0.3 \pm 0.5$
$\chi_{c2} \to \phi\phi$	...	...	$10.7 \pm 0.3 \pm 1.2$
$\chi_{c0} \to \omega\omega$	991 ± 38	13.1	$9.5 \pm 0.3 \pm 1.1$
$\chi_{c1} \to \omega\omega$	597 ± 29	13.2	$6.0 \pm 0.3 \pm 0.7$
$\chi_{c2} \to \omega\omega \to 2(\pi^+\pi^-\pi^0)$	762 ± 31	11.9	$8.9 \pm 0.3 \pm 1.1$
$\chi_{c0} \to \omega\phi$	76 ± 11	14.7	$1.2 \pm 0.1 \pm 0.2$
$\chi_{c1} \to \omega\phi$	15 ± 4	16.2	$0.22 \pm 0.06 \pm 0.02$
$\chi_{c2} \to \omega\phi \to K^+K^-\pi^+\pi^-\pi^0$	<13	15.7	<0.2

The uncertainties due to the modified χ_{cJ} MC shapes are estimated by replacing them with Breit-Wigner functions convolved with the instrumental resolution functions in the fits. The quality of the resulting fit is not as good as using the modified MC shapes. The difference of signal yields varies from 1% to 4%, and this is included as a systematic error.

The detection efficiencies are determined from MC simulations for the sequential decays $\psi(3686) \to \gamma\chi_{cJ} \to VV$, V decays into the selected final state. The decays $\psi(3686) \to \gamma\chi_{cJ}$ are generated by assuming a pure $E1$ transition. The $\chi_{cJ} \to VV$ decays and subsequent decays of the V are modeled with helicity amplitudes that provide angular distributions consistent with the data.

The systematic uncertainties on the χ_{cJ} decay branching fractions arise from the $\pi^\pm$ and $K^\pm$ tracking, $K^\pm$ identification, EMC shower reconstruction, number of $\psi(3686)$ decays, kinematic fitting, modified MC shapes, background estimation, χ_{cJ} signal extraction and uncertainties from branching fractions of $\psi(3686) \to \gamma\chi_{cJ}$, $\phi \to K^+K^-$, $\omega \to \pi^+\pi^-\pi^0$ and $\pi^0 \to \gamma\gamma$. The uncertainties caused by MDC tracking are estimated to be 2% for each charged track [17]. The uncertainty due to $K^\pm$ identification is evaluated to be 2% per kaon [17]. The uncertainty due to the photon reconstruction is determined to be 1% for each photon [17]. The uncertainty in the number of $\psi(3686)$ decays is 4% [12]. The uncertainties due to the kinematic fit are determined by comparing the efficiency at the given χ^2_{4C} values for the MC sample to control samples selected from data, i.e., $\psi(3686) \to \gamma\phi\phi \to \gamma 2(K^+K^-)$, $\psi(3686) \to \pi^0\pi^0 J/\psi$, $J/\psi \to 2(\pi^+\pi^-)$, $\pi^0 2(\pi^+\pi^-)$ and $\psi(3686) \to \pi^+\pi^- J/\psi$, $J/\psi \to K^+K^-\pi^0$. The kinematic-fit uncertainty varies from 0.5% ($\gamma 2(\pi^+\pi^-\pi^0)$ mode) to 3.7% ($\gamma K^+K^-\pi^+\pi^-\pi^0$ mode). The uncertainties of the peaking backgrounds for $\chi_{cJ} \to \phi\phi \to 2(K^+K^-)$ are evaluated by comparing the sideband estimates to the exclusive MC simulation on the modes $\chi_{cJ} \to \phi K^+K^-$ and $2(K^+K^-)$, while for other modes the uncertainties are estimated by varying the size of sideband boxes. The uncertainties of the peaking background estimates are less than 3%. The uncertainty from the MC normalization factor is found to be negligibly small. The total systematic uncertainties are 10% for $\chi_{cJ} \to \phi\phi \to 2(K^+K^-)$ mode, and 11% for $\chi_{cJ} \to \omega\omega \to 2(\pi^+\pi^-\pi^0)$, $\chi_{cJ} \to \phi\phi$, $\omega\phi \to K^+K^-\pi^+\pi^-\pi^0$ modes.

The branching fractions for χ_{cJ} decays are determined from $\mathcal{B} = N_{\rm net}/(N_{\psi'}\epsilon\prod_i \mathcal{B}_i)$, where $N_{\rm net}$ and ϵ are the number of net signal events and the detection efficiency, respectively. The detection efficiencies are listed in Table I. Here $N_{\psi'} = (106 \pm 4) \times 10^6$ [12] is the number of $\psi(3686)$ events, and $\prod_i \mathcal{B}_i$ is the product of world average branching fractions values [15] for $\psi(3686) \to \gamma\chi_{cJ}$ and the other meson decays that are involved. For the $\chi_{cJ} \to \phi\phi \to K^+K^-\pi^+\pi^-\pi^0$ branching fraction we double the efficiency listed in Table I since our analysis sums over the two combinations for each ϕ to decay to either K^+K^- or $\pi^+\pi^-\pi^0$. The resulting branching fractions are listed in Table I. The statistical significance of $\chi_{cJ} \to \omega\phi$ is derived from the change of $-2\ln\mathcal{L}$ obtained from fits with and without each of the three $\chi_{cJ} \to \omega\phi$ signal components. We obtain a significance of 4.1σ for $\chi_{c1} \to \omega\phi$ and 1.5σ for $\chi_{c2} \to \omega\phi$. The significance of the $\chi_{c0} \to \omega\phi$ signal is 10σ. Using the Bayesian method, the upper limit for the number of signal events of the $\chi_{c2} \to \omega\phi$ mode is 13 at the 90% confidence level (C.L.). The branching fractions for $\chi_{cJ} \to \phi\phi$ measured in $2(K^+K^-)$ and $(K^+K^-)(\pi^+\pi^-\pi^0)$ final states are combined into a weighted average, where common systematic uncertainties are counted only once.

In summary, the HSR suppressed decays of $\chi_{c1} \to \phi\phi$, $\omega\omega$, and the doubly OZI-suppressed decay $\chi_{c0} \to \omega\phi$ are observed for the first time. The branching fractions are measured to be $(4.4 \pm 0.3 \pm 0.5) \times 10^{-4}$, $(6.0 \pm 0.3 \pm 0.7) \times 10^{-4}$, and $(1.2 \pm 0.1 \pm 0.2) \times 10^{-4}$, for $\chi_{c1} \to \phi\phi$, $\omega\omega$, and $\chi_{c0} \to \omega\phi$, respectively, We also find evidence for $\chi_{c1} \to \omega\phi$ decay with a signal significance of 4.1σ. The branching fractions for $\chi_{c0/2} \to \phi\phi$, $\omega\omega$ decays are remeasured with a precision that is better than those of the current world average values [15]. These precise measurements will be helpful for understanding χ_{cJ} decay mechanisms. In particular, the measured branching fractions for $\chi_{c1} \to VV$ indicate that HSR is significantly violated and that long-distance effects play an important role in this energy region. The long-distance effects from the intermediate charmed meson loops in $\chi_{c1} \to \phi\phi$ and $\omega\omega$ decays [7,8] can contribute to the branching fractions at the level of 10^{-4} but are more than an order of magnitude too small to explain the doubly OZI-suppressed decay rate for $\chi_{c1} \to \omega\phi$ that we measure [8].

We thank the accelerator group and computer staff of IHEP for their effort in producing beams and processing data. We are grateful for support from our institutes and universities and from these agencies: Ministry of Science and Technology of China, National Natural Science Foundation of China, Chinese Academy of Sciences, Istituto Nazionale di Fisica Nucleare, Russian Foundation for Basic Research, Russian Academy of Science (Siberian branch), U.S. Department of Energy, and National Research Foundation of Korea.

[1] A. Duncan, A. Mueller, Phys. Lett. B **93**, 119 (1980); H. F. Jones, J. Wyndham, Nucl. Phys. **B195**, 222 (1982); M. Anselmino, F. Murgia, Phys. Rev. D **47**, 3977 (1993).
[2] J. Bolz, P. Kroll, and G. A. Schuler, Eur. Phys. J. C **2**, 705 (1998); S. M. H. Wong, Eur. Phys. J. C **14**, 643 (2000).
[3] M. Ablikim *et al.* (BES Collaboration), Phys. Lett. B **642**, 197 (2006).
[4] M. Ablikim *et al.* (BES Collaboration), Phys. Lett. B **630**, 7 (2005).
[5] H. Q. Zhou, R. G. Ping, and B. S. Zou, Phys. Lett. B **611**, 123 (2005).
[6] S. J. Brodsky and G. P. Lepage, Phys. Rev. D **24**, 2848 (1981).
[7] Xiao-Hai Liu and Qiang Zhao, Phys. Rev. D **81**, 014017 (2010).
[8] Dian-Yong Chen, Jun He, Xue-Qian Li, and Xiang Liu, Phys. Rev. D **81**, 074006 (2010).
[9] M. Ablikim *et al.* (BES Collaboration), Nucl. Instrum. Methods Phys. Res., Sect. A **614**, 345 (2010).
[10] S. Agostinelli, *et al.* (GEANT4 Collaboration), Nucl. Instrum. Methods Phys. Res., Sect. A **506**, 250 (2003).
[11] J. Allison, *et al.* IEEE Trans. Nucl. Sci. **53**, 270 (2006).
[12] M. Ablikim *et al.* (BES Collaboration), Phys. Rev. D **81**, 052005 (2010).
[13] Kuang-Ta Chao and Yifang Wang, Int. J. Mod. Phys. A **24**, Supp. 1 (2009), http://www.worldscinet.com/ijmpa/24/24supp01/S0217751X0924supp01.html.
[14] D. J. Lange, Nucl. Instrum. Methods Phys. Res., Sect. A **462**, 152 (2001).
[15] K. Nakamura *et al.* (Particle Data Group), J. Phys. G **37**, 075021 (2010).
[16] W. Verkerke and D. P. Kirkby, arXiv:physics/0306116.
[17] M. Ablikim *et al.*, (BES Collaboration), Phys. Rev. D **83**, 112005 (2011).